Journal of Mines, Metals and Fuels, *71(10): 1754-1763; 2023. DOI: 10.18311/jmmf/2023/35052*

Print ISSN : 0022-2755

Journal of Mines, Metals and Fuels

Contents available at: *www.informaticsjournals.com/index.php/jmmf*

Impact of Flow, Heat and Mass Transfer of Newtonian and Non-Newtonian Nanofluids Flow over a Non-Darcy Stretching Sheet in the Context of Fuel Applications

C. Manoj Kumar and A. Jasmine Benazir*

Department of Mathematics, Presidency University, Rajanukunte, Yelahanka, Bengaluru -560064, Karnataka, India; mngowda9676@gmail.com, jasminebenazir@gmail.com

Abstract

The study of flow, heat, and mass transfer of Newtonian and non-Newtonian nanofluid over porous media holds paramount significance in the context of fuel industries, contributing to enhanced efficiency, reduced emissions, and sustainable energy production. This investigation provides a concise overview of the critical role played by porous media in various aspects of the fuel sector. In the oil and gas industry, porous reservoir formations exhibit complex fluid dynamics characterized by non-Darcy flow, influencing recovery rates of hydrocarbons. Understanding the relationship between flow, heat, and mass transfer within these porous reservoirs is essential for reservoir engineers and fuels the quest for maximizing resource extraction. The Sisko nanofluid model is one of the most sought-after mathematical model which prophesies the interesting features of Newtonian and non-Newtonian (dilatant and Pseudoplastic nature) fluids. In contemporary years, a new class of non-Newtonian fluids with nanoparticle suspensions are gaining popularity as it is beneficial in enhancing thermal efficiency in several applications such as warming/cooling of home appliances and micro-electronics etc. However, the modeling on this class of non-Newtonian fluids is limited. In light of above, this work predicts the stream, heat and mass transmission behavior of nanofluids using Sisko fluid model. Stretching sheet with porous medium has been used for this study with addition with magnetic field, thermal radiation, Brownian motion and thermophoresis. The non-linearity issues in this fluid flow are addressed in the prevailing work using suitable similarity transformations. The non-linear dimensional coupled P.D.E are converted into nonlinear dimensionless coupled O.D.E. These equations are solved using MATLAB by implementing four-stage Lobatto IIIa formula. The impacts of copious physical parameters of flow, energy and mass transfer insights are discussed. From the outcomes of current work, it is perceived that increasing the perviousness of the porous medium reduces the fluid mobility. Further, for increased values of Prandtl number the heat transfer coefficient increases ensuing in more heat transfer. Flow, heat, and mass transfer over porous media are integral to fuel industries, influencing resource extraction, energy conversion, and product quality.

Keywords: *Heat Transfer, Mass Transfer, Porous Medium, Sisko Nanofluid, Stretching Sheet*

1.0 Introduction

In the pursuit of enhanced efficiency, sustainability, and innovation in both the metal and fuel industries, the intricate study of fluid dynamics, heat transfer, and mass transport has emerged as a focal point of research and development. Momentum and thermal boundary layer stream over a linear enlarging surface is scrutinized by Chaim[1]. The mass as well as heat transmission of an electrically conducting nanofluid through a permeable stretched sheet have been addressed by Yirga and Tesfay[2]. By combining the FDM with quasilinearization approach, Bisht and Sharma[3] have achieved substantial advance in their knowledge of the special characteristics

*Author for correspondence

of entropy formation in the flow and heat exchange of Sisko nanofluid over a stretched surface. Khan *et al*.,[4] have reported a relative research of shooting method and HAM with convective boundary conditions over an elongating sheet. The significant outcomes are found to be in good agreement with both the methods. It is also found that the thermal boundary thickness enhances with intensifying the convective heat transfer coefficients. Numerous researchers have reported the boundary layer flow non-Newtonian fluids[5-8]. Based on viscosity, fluids can be classified as Newtonian fluids and non-Newtonian fluids. The stress tensor and velocity gradients are in linear relationship for Newtonian fluids. Whereas, for non-Newtonian fluids the relation is always non-linear. Several significant examples of non-Newtonian fluids that can be discussed in this context include Polyethylene, thermoplastics, granular substances, resin, colorants, asphalt, gel, and organic fluids. Mathematically, it is difficult to obtain exact solutions for non-Newtonian fluids, because of its non-linearity. There are several existing models that can be implemented for modelling non-Newtonian fluids, which include the Sisko fluid model, the Eyring-Powell fluid model, the Carreau fluid model, and the Maxwell fluid model. However, Sisko fluid model is quite popular as it addresses the nonlinearity issues in non-Newtonian fluids.

The present study focusses on Sisko fluid model, since these models characterize the both Newtonian fluids and non-Newtonian fluids (Shear thickening and thinning fluids). In 1957, Sisko[9] has proposed this model, taking grease as a relevant example. These fluid model have wide range of applications in blood simulation, mixing of paints and lubricating nanofluid etc. Khan and Shahzad[10] have made significant progress in analyzing the boundary layer theory of Sisko nanofluid over a stretching sheet. Bisht and Sharma[3] have scrutinized entropy generation in electrically conducting Sisko nanofluid over stretching surface. There are numerous studies that have reported the boundary layer's theory of flow, heat and mass transport features in Sisko nanofluids[11-15].

Non-Darcy porous medium flow refers to fluid flow through porous materials where the flow behavior deviates from Darcy's law, which describes flow through porous media as directly proportional to the pressure gradient. Non-Darcy flow is typically encountered in situations where the flow velocities are relatively high, the pore structure is complex, or the fluid properties are non-Newtonian. In the context of fuel industries, there are several applications where non-Darcy flow phenomena can be observed. For examples, in the oil and gas industry, porous reservoir formations exhibit complex fluid dynamics characterized by non-Darcy flow, influencing hydrocarbon recovery rates. Understanding the interplay between flow, heat, and mass transfer within these porous reservoirs is pivotal for reservoir engineers and fuels the quest for maximizing resource extraction. The Coalbed Methane (CBM) industry encounters non-Darcy flow within coal seams. Understanding these flow characteristics is critical for optimizing methane extraction. Processes like coal gasification and biomass pyrolysis involve complex flow in porous beds, were non-Darcy flow behavior influences gas yield and product quality. Fractured reservoirs exhibit non-Darcy flow behavior due to fractures and fissures. This is particularly relevant for Enhanced Oil Recovery (EOR) techniques, where non-Darcy flow affects the efficiency of recovery methods[16-20].

Rapid heat transfer has been a topic of interest for expanding engineering fields during the past ten years. Attempts are being made to continuously to enhance the amount of heat transmission and heat conductivity, along with works to moderate frictional loss, pressure drop, and pumping power associated with the heat transfer fluid. The term "nanofluid" denotes a novel category of heat transfer fluids that have been formulated to exhibit improved thermal properties for usage of heat conduction. A tiny number of nanoparticles are suspended in base fluids like water, ethylene glycol, etc to create nanofluid, either with or without stabilization methods. Nanoparticles typically have a size of less than 100 nm[21-27].

2.0 Development of the Problem

Consider the steady state 2-D electrical conducting fluid flow of incompressible Sisko nanofluid over a porous extending sheet as depicted in Figure 1. The nanofluids flow along the x-axis with the velocity component u while v is the velocity component considered along y-axis.

The stretching sheet has been accelerated with uniform velocity U_w=cx along the horizontal direction, where c be the non-zero positive real number. A uniform magnetic field B_0 is pertained perpendicular to the

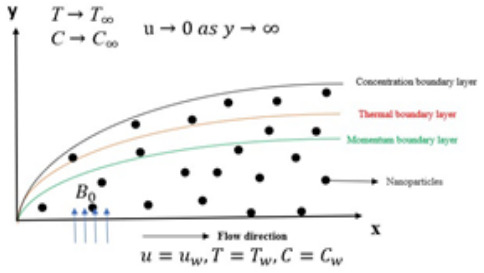

Figure 1. Geometry of the flow problem.

surface assuming non-Darcy porous permeable medium in momentum equation. The energy and concentration equations are explored with the mechanism of thermal conductivity (of nanoparticle and its base fluids), thermal radiation, Brownian motion and thermophoresis with 1st - order chemical reactions. The surface of the elongating sheet is retained at a constant temperature T_w and concentration C_w near the surface. In addition, T_∞ and C_∞ are free stream temperature, free stream concentration respectively. Based on above stated assumptions, the boundary layer flow of the governing equations may be described as follows.

$$\frac{\partial u}{\partial x}+\frac{\partial v}{\partial y}=0 \tag{1}$$

$$u\frac{\partial u}{\partial x}+v\frac{\partial u}{\partial y}=\frac{a}{\rho_{nf}}\frac{\partial^2 u}{\partial y^2}-\frac{b}{\rho_{nf}}\frac{\partial}{\partial y}\left(-\frac{\partial u}{\partial y}\right)^n-\frac{\sigma B_0^2 u}{\rho_{nf}}-\frac{\mu}{\rho_{nf}K}u-\frac{C_b}{\sqrt{K}}u^2 \tag{2}$$

$$u\frac{\partial T}{\partial x}+v\frac{\partial T}{\partial y}=\alpha\left(\frac{\partial^2 T}{\partial x^2}+\frac{\partial^2 T}{\partial y^2}\right)-\frac{1}{(\rho c_p)_{nf}}\left(\frac{\partial q_r}{\partial y}\right)+\tau\left[D_B\left(\frac{\partial C}{\partial y}\right)\left(\frac{\partial T}{\partial y}\right)+\frac{D_T}{T_\infty}\left(\frac{\partial T}{\partial y}\right)^2\right] \tag{3}$$

$$u\frac{\partial C}{\partial x}+v\frac{\partial C}{\partial y}=D_B\frac{\partial^2 C}{\partial y^2}+\frac{D_T}{T_\infty}\frac{\partial^2 T}{\partial y^2}-K_r(C-C_\infty) \tag{4}$$

The appropriate boundary constraints for the eqns. (1) – (4) are as follows:

$$u=U_w=cx, v=0, T=T_w, C=C_w \quad at y=0 \tag{5}$$

$$u\to 0, T\to T_\infty, C\to C_\infty, at\ y\to\infty \tag{6}$$

Using Rosseland[28] approximation, the thermal radiation can be written as

$$q_r=-\frac{4\sigma^*}{3k^*}\frac{\partial T^4}{\partial y}$$

The P.D. Es to O.D. Es conversion is carried out using the similarity transformations listed below for the purpose of mathematical examination of the problem.

$$u=cxf'(\eta),$$

$$v=-u_w Re_b^{-\frac{2}{n+1}}\frac{1}{n+1}\left[2nf(\eta)+(1-n)\eta f'^{(\eta)}\right],$$

$$\eta=\frac{y}{x}Re_b^{\frac{1}{n+1}} \tag{7}$$

$$\theta(\eta)=\frac{T-T_\infty}{T_w-T_\infty},\ \phi(\eta)\frac{C-C_\infty}{C_w-C_\infty} \tag{8}$$

$$Af'''(\eta)+n\left(-f''(\eta)\right)^{(n-1)}f'''(\eta)-Mf'(\eta)-(f(\eta))^2+\frac{2n}{n+1}f(\eta)f''(\eta)-\varphi f'-F(f(\eta)=0 \tag{9}$$

$$(1+R)\theta''(\eta)+P_r\frac{2n}{n+1}f(\eta)\theta'(\eta)+N_B\theta'(\eta)\phi'(\eta)+N_T(\theta'(\eta))^2=0 \tag{10}$$

$$\phi''(\eta)+\frac{N_T}{N_B}\theta''(\eta)-LeP_r\left(-\frac{2n}{n+1}f(\eta)\phi'(\eta)+\sigma\phi(\eta)\right)=0 \tag{11}$$

The appropriate boundary conditions of Eqns. (9) – (11) are followed by:

$$f(0)=0, f'(0)=1, \theta(0)=1, \qquad \phi(0)=1, at\ \eta=0 \tag{12}$$

$$f'(\infty)\to 0, \theta(\infty)\to 0, \phi(\infty)\to 0\ at\ \eta\to\infty \tag{13}$$

Where the non-dimensional parameters are

$$A=\frac{Re_b^{\frac{2}{n+1}}}{Re_a}, M=\frac{{B_0}^2\sigma\, x}{u_w\rho_{nf}}$$

$$Re_a=\frac{\rho_{nf}xu_w}{\mu_a}, Re_b=\frac{\rho_{nf}x^n{u_w}^{2-n}}{b}, \varphi=\frac{\nu_{nf}}{Kc}, P_r=\frac{xu_w}{\alpha Re_b^{\frac{2}{n+1}}}$$

$$R=\frac{16\sigma^* T_\infty^3}{3kk^*}, N_B=\frac{\tau D_B}{\alpha}(C_w-C_\infty), \alpha=\frac{K}{\rho_{nf}c_p},$$

$$N_T=\frac{\tau D_T}{\alpha T_\infty}(T_w-T_\infty), \sigma=\frac{K_r}{c}, L_B=\frac{\alpha}{D_m}, F=\frac{C_b x}{\sqrt{K}}$$

The dimensionless physical quantities of interest are the Cf_x, Nu_x, Sh_x which are mathematically denoted as:

$$Cf_x = \frac{2\tau_w}{\rho u_w{}^2},\ Nu_x = \frac{x q_w|_{y=0}}{K(T_w - T_\infty)},\ Sh_x = \frac{x j_w|_{y=0}}{D_B(C_w - C_\infty)} \quad (14)$$

τ_w, q_w, j_w and are the stress tensor, heat flux and mass flux respectively, and are defined as

$$\tau_w = \left(a - b\left|-\frac{\partial u}{\partial y}\right|^{n-1}\right)\frac{\partial u}{\partial y}$$

$$q_w = -K\left(\frac{\partial T}{\partial y}\right),\ j_w = -D_B\left(\frac{\partial C}{\partial y}\right) \quad (15)$$

Using Eqns. (7) and (8), the output of solutions of dimensionless physical quantities are shown below and their variations with pertinent physical parameters are tabulated.

$$\frac{1}{2} Re_b{}^{\frac{1}{n+1}} C_f = A f''(0) - (-f''(0))^n \quad (16)$$

$$Re_b{}^{-\frac{1}{n+1}} Nu_x = -\theta'(0), \quad (17)$$

$$Re_b{}^{-\frac{1}{n+1}} Sh_x = -\phi'(0) \quad (18)$$

3.0 Solution Methodology

The solutions of above-mentioned governing coupled O.D. Es. (9) – (11) with boundary constraints (12) and (13) are computed with four-stage Lobatto IIIa formula using MATLAB. This formula is used to solve ordinary differential equations with high convergence obtaining solutions close to exact solutions. To achieve the numerical solutions, the boundary valued problems have been converted to initial valued problem by assigning the new variables to higher order terms, then initializing the arbitrary initial guesses to satisfy the estimated error tolerance.

$$f = f_1, f' = f_2, f'' = f_3, \theta = f_4, \theta' = f_5, \phi = f_6, \phi' = f_7$$

4.0 Result and Discussions

In this section, the impact of different physical factors on flow, energy and mass transfer attributes are demonstrated through graphs as well as tables by fixing values of n=4, A=0.5, M=0.4, φ=0.005, F=0.02, P_r=0.7, R=0.3, N_T=0.2, N_B=0.3, σ=0.2, L_e=0.5. The following default values are set for the governing parameters based on the previous investigations.

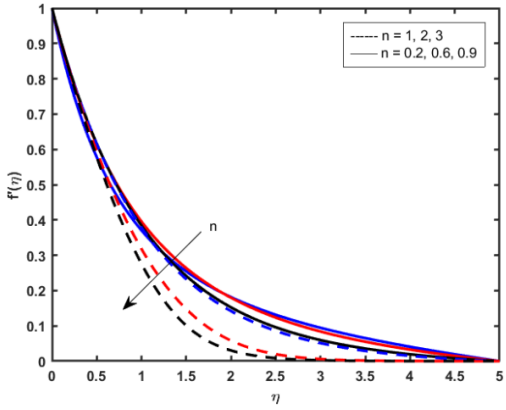

Figure 2. Impact of n on velocity profile.

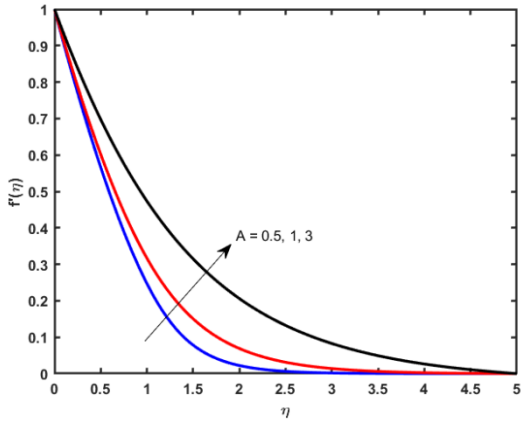

Figure 3. Impact of A on velocity profile.

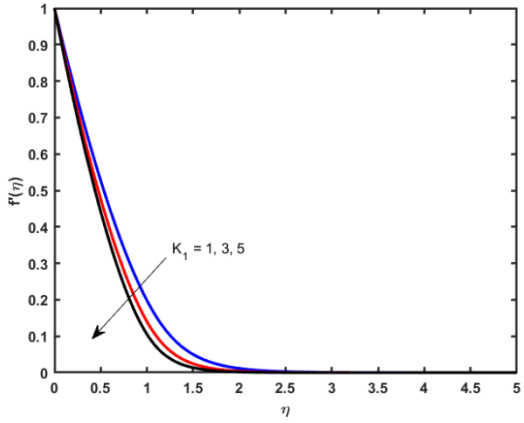

Figure 4. Impact of K_1 on velocity profile.

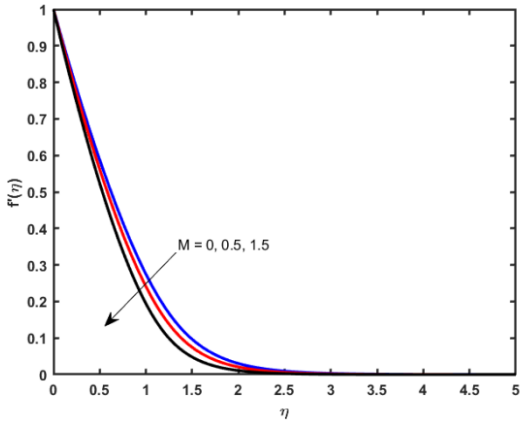

Figure 5. Impact of M on velocity profile.

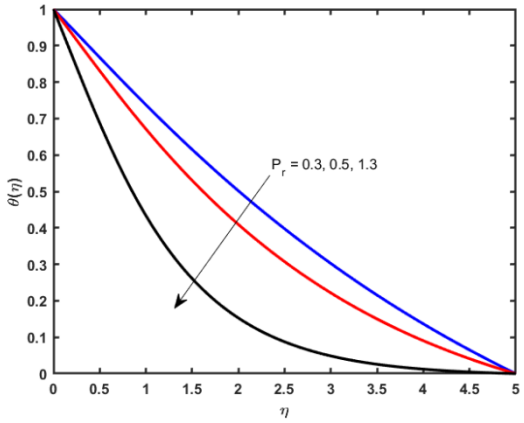

Figure 6. Impact of P_r on temperature profile.

Figures 2-5, illustrate the influence of distinct values of various physical parameters over the momentum boundary layer thickness. From Figure 2, it is witnessed that strengthening the flow index value (n) decelerates the fluid flow. In general, this is because provoking the n value stimulates the fluid viscosity, which interrupts the fluid flow. Figure 2 also demonstrates the momentum boundary layer thickness of both shear thickening and thinning (1<n>1). Solid line represents the shear thickening fluids and doted lines represents the shear thinning fluids. It is to be noted that the fluids flow takes place faster for n<1.

Figure 3 shows that the variation of Sisko nanofluid parameter (A) on momentum boundary layer thickness. It is observed that intensifying values of A enhances the fluid mobility thereby enhancing the velocity profile. The fluctuation of permeability parameter (K_1) on the velocity pattern is apparent in Figure 4. It becomes evident that the velocity field is a diminishing function of the porosity parameter K_1. Physically, a spike in porosity K_1 causes the permeability to decline, which causes an erosion in the velocity distribution. In general, these kinds of results significant in fuel industries to extract the fuels with nanoparticle suspensions. The behavior of the magnetic field parameter (M) on the velocity profile is shown in Figure 5. It is important to note that the Lorentz forces in the electrically conducting fluids cause the transverse magnetic field to lower the fluid velocity inside the momentum boundary layer. As a result of this Lorentz force's resistance to fluid motion, the velocity profile slows down. Figure 6 depicts the variance in temperature

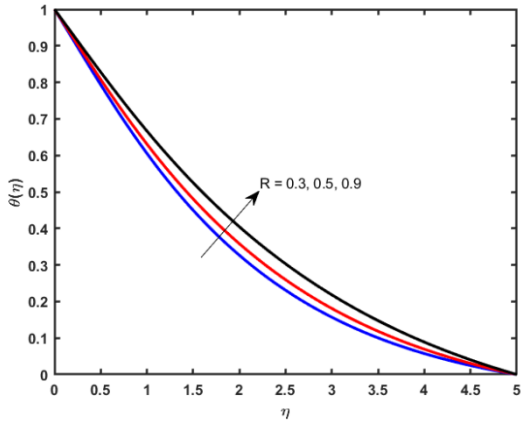

Figure 7. Effect of R on Temperature profile.

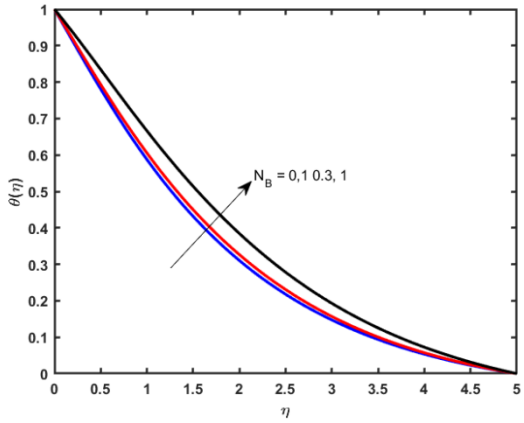

Figure 8. Impact of N_B on temperature profile.

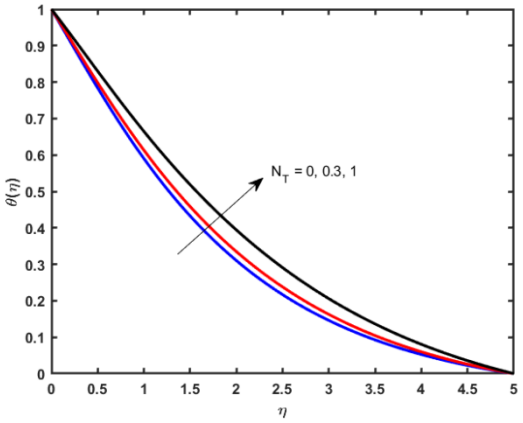

Figure 9. Impact of N_T on temperature profile.

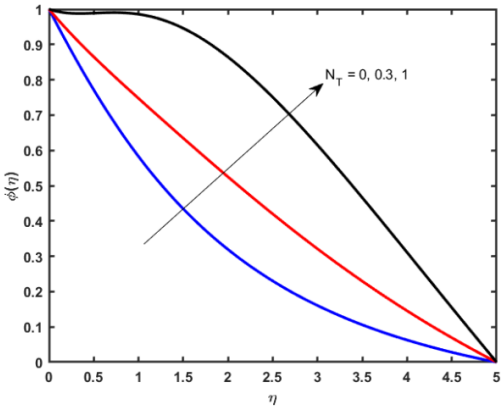

Figure 10. Effect of N_T on mass transfer profile.

distribution for various values of the Prandtl number. The lower temperature distribution is caused by higher values of Prandtl number (Pr). In general, enhanced Pr values are associated with reduced conductivity of heat, which triggers the reduction in fluid temperature distribution. From Figure 7, propelling values of the radiation of heat parameter (R) accelerates the heat conduction at the surface, which leads to upsurge in the thermal boundary layer thickness.

The temperature difference caused due changes in N_T and N_B are observed from Figure 8 and 9. Strengthening the N_T and N_B parameters leads to greater particle mobility, enhanced mixing, and improved heat transfer within the fluid near the solid surface. These effects

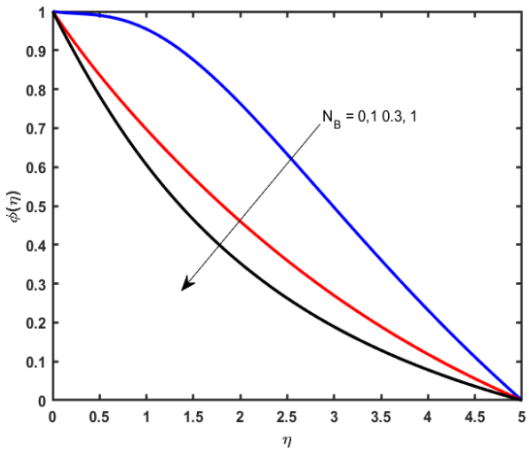

Figure 11. Influence of N_B on Mass transfer profile.

collectively result in a thicker thermal boundary layer. Augmenting the thermophoresis parameter augments the mass transfer process due to its influence on particle motion in response to temperature gradients. As the N_T upsurges, particles suspended in the fluid experience stronger thermophoretic forces, prompting them to migrate towards regions with temperature variations. This migration of particles enhances their contact with the surrounding fluid, facilitating a more efficient mass transfer process. Consequently, the amplified values of N_T leads to a greater concentration which is shown in Figure 10. From Figure 11, it is observed that escalating values of N_B decelerates the mass trasmission.

Table 1. Validation of solutions for Local Skin frction compare with previous existing works

A	n	Khan and Shahzad[1]	Present Result
1	1	-1.414214	-1.424630
	2	-1.343198	-1.344313
	3	-1.311338	-1.312145
0	1	-1	-1.001396
1		-1.414214	-1.424630
2		-1.732051	-1.760840

Table 1, reports that there is a good agreement in comparison of local Skin friction for distinct values of **A** and **n** with the works of M. Khan and A. Shahzad[10]. For fixed values of M=0, =0, F=0, P_r=0, R=0, N_T=10^{-6}, N_B=10^{-6}, σ =0, L_e=0.

Table 2. Variation of C_{fx}, Nu_x and, Sh_x of various physical parameters

n	M	φ	F	A	R	σ	L_e	P_r	N_T	N_B	$\frac{1}{2}Re_b^{\frac{1}{n+1}}C_f$	-θ' (0)	-ϕ' (0)
0.2 0.6 0.9	0.4	0.005	0.02	0.5	0.3	0.2	0.5	0.7	0.2	0.3	-1.658628 -1.533699 -1.474097	0.217563 0.300644 0.336235	0.366531 0.364523 0.363307
1 2 3											-1.459575 -1.385021 -1.355084	0.344662 0.386846 0.403006	0.362996 0.360796 0.359640
4	0 0.5 1.5										-1.124481 -1.390102 -1.878154	0.422504 0.409315 0.390860	0.358923 0.358999 0.359615
		1 3 5									-1.829237 -2.709266 -3.508551	0.392453 0.369393 0.355149	0.359522 0.360917 0.362029
			0.5 0.61 0.7								-1.496691 -1.532301 -1.561264	0.407593 0.406721 0.406023	0.359079 0.359106 0.359129
				0.5 1 3							-1.338395 -1.536767 -2.286140	0.411670 0.438580 0.497825	0.358962 0.360064 0.371205
					0.3 0.5 0.9						-1.338395 -1.338395 -1.338395	0.411670 0.383022 0.343354	0.358962 0.377231 0.402695
						0 0.4 0.8					-1.338395 -1.338395 -1.338395	0.417757 0.407108 0.400655	0.221272 0.472636 0.655883
							0.22 0.96 2				-1.338395 -1.338395 -1.338395	0.422034 0.399913 0.386441	0.187758 0.607508 1.045541
								0.3 0.5 1.3			-1.338395 -1.338395 -1.338395	0.261498 0.335270 0.631229	0.290688 0.326284 0.458048
									0 0.3 1		-1.338395 -1.338395 -1.338395	0.434752 0.400480 0.328428	0.490584 0.303440 0.087968
										0.1 0.3 1	-1.338395 -1.338395 -1.338395	0.444723 0.411670 0.309429	0.033568 0.358962 0.471745

Table 2, reports that the influences of various physical parameters on C_{fx}, Nu_x and, Sh_x. Intensifying the values of flow index value (n) increases the viscosity of the fluids, which in turn strengthens the Skin friction factor for both thickening and thinning fluids. Heat transfer coefficient (Nusselt number) stimulates the viscosity of the fluids but declines the mass transfer coefficient. Intensifying values of magnetic field, Forcheimmer porous medium parameter and Sisko nanofluid parameters decline C_{fx} coefficient. Local Nu_x number strengthens for augmenting

values of material parameter and Prandtl numbers. Mass transfer coefficient i.e., local Sh_x deteriorates for increased values of Brownian diffusion, radiation, Schmidt number and Prandtl number parameters.

5.0 Conclusions

This paper presents a numerical investigation of flow, heat and mass transfer of Sisko nanofluid over a non-Darcy surface with the effects of magnetic field, thermal radiation, Brownian diffusion and molecular diffusion.

The significant outcomes of the flow problem studied in the present work are as follows.

1. Fluid velocity reduces for intensifying values of n (1<n>1), magnetic field, porous medium parameters.
2. Local Cf_x coefficient strengthens for augmenting values of powerlaw index parameter for both Dilatant and Pseudoplastic fluids.
3. Energy profile proliferates for supplementing values of thermal radiation, Brownian diffusion and molecular diffusion coefficients.
4. Heat transfer coefficient and mass transfer coefficient strengthens for higher values of Pr.
5. Mass transfer profile intensifies for higher values of molecular diffusion whereas for Brownian diffusion it shows a contrary nature.

The non-Darcy porous medium flow plays a significant role in various aspects of the fuel industry, from reservoir engineering to fuel cell technology and biofuel production. Accurate modeling and characterization of non-Darcy flow are essential for improving efficiency, optimizing processes, and ensuring the sustainability of fuel production and utilization.

6.0 References

1. Chiam TC. Heat transfer in a fluid with variable thermal conductivity over a linearly stretching sheet. Acta Mech. 1998; 129(1-2):63-72. https://doi.org/10.1007/BF01379650
2. Yirga Y, Tesfay D. Heat and Mass Transfer in MHD Flow of Nanofluids through a Porous Media Due to a Permeable Stretching Sheet with Viscous Dissipation and Chemical Reaction Effects. Int J Mech Mechatronics Eng. 2015 Apr 4; 9(5):709-16. https://doi.org/10.1080/15502287.2015.1048385
3. Bisht A, Sharma R. Entropy generation analysis in magnetohydrodynamic Sisko nanofluid flow with chemical reaction and convective boundary conditions. Math Methods Appl Sci. 2021; 44(5):3396-417. https://doi.org/10.1002/mma.6948
4. Khan M, Malik R, Munir, Shahzad A. MHD flow and heat transfer of Sisko fluid over a radially stretching sheet with convective boundary conditions. J Brazilian Soc Mech Sci Eng. 2016; 38(4):1279-89. https://doi.org/10.1007/s40430-015-0437-y
5. Prasad KV, Vajravelu K, Vaidya H, Raju BT. Heat Transfer in a Non-Newtonian Nanofluid Film Over a Stretching Surface. J Nanofluids. 2015; 4(4):536-47. https://doi.org/10.1166/jon.2015.1174
6. Sivaraj R, Banerjee S. Transport properties of non-Newtonian nanofluids and applications. Eur Phys J Spec Top. 2021; 230:1167-71. https://doi.org/10.1140/epjs/s11734-021-00031-1
7. Van Canneyt K, Verdonck P. Mechanics of Biofluids in Living Body. Compr Biomed Phys. 2014; 10:39-53. https://doi.org/10.1016/B978-0-444-53632-7.01003-0
8. Zheng L, Zhang X. Exact Analytical Solutions for Fractional Viscoelastic Fluids. Model Anal Mod Fluid Probl. 2017; pp. 279-359. https://doi.org/10.1016/B978-0-12-811753-8.00007-4
9. Sisko AW. The Flow of Lubricating Greases. Ind Eng Chem. 1958; 50(12):1789-92. https://doi.org/10.1021/ie50588a042
10. Khan M, Shahzad A. On boundary layer flow of a Sisko fluid over a stretching sheet. Quaest Math. 2013; 36(1):137-51. https://doi.org/10.2989/16073606.2013.779971
11. Ge-Jile H, Waqas H, Khan SU. Khan MI, Farooq S, Hussain S. Three-dimensional radiative bioconvective flow of a sisko nanofluid with motile microorganisms. Coatings. 2021; 11(3):335. https://doi.org/10.3390/coatings11030335
12. Malik R, Khan M, Mushtq M. Cattaneo-Christov heat flux model for Sisko fluid flow past a permeable nonlinearly stretching cylinder. J Mol Liq. 2016; 222:430-4. https://doi.org/10.1016/j.molliq.2016.07.040
13. Al-Mamun A, Arifuzzaman SM, Reza-E-Rabbi K, Biswas P, Khan MS. Computational modelling on MHD radiative sisko nanofluids flow through a nonlinearly stretching sheet: Int J Heat Technol. 2019; 37(1):285-95. https://doi.org/10.18280/ijht.370134

14. Jawad M, Shah Z, Islam S, Khan W, Khan AZ. Nanofluid thin film flow of Sisko fluid and variable heat transfer over an unsteady stretching surface with external magnetic field. J Algorithm Comput Technol. 2019; 13:174830181983245. https://doi.org/10.1177/1748301819832456
15. Pal D, Mandal G. Magnetohydrodynamic stagnation-point fl ow of Sisko nano fluid over a stretching sheet with suction. Propuls Power Res. 2020; 9(4):408-22. https://doi.org/10.1016/j.jppr.2020.06.002
16. Jasmine Benazir A, Sivaraj R. Influence of Double Dispersion on Non-Darcy Free Convective Magnetohydrodynamic Flow of Casson Fluid. Adv Intell Syst Comput. 2016; 436:537-51. https://doi.org/10.1007/978-981-10-0448-3_44
17. Shankar DG, Raju C S K, Kumar M SJ, and Makinde OD. Cattaneo-christov heat flux on an MHD 3D free convection casson fluid flow over a stretching sheet. Eng Trans. 2020; 68(3):223-38.
18. Nithiarasu P, Seetharamu KN, Sundararajan T. Natural convective heat transfer in a fluid saturated variable porosity medium. Int J Heat Mass Transf. 1997; 40(16):3955-67. https://doi.org/10.1016/S0017-9310(97)00008-2
19. Shenoy AV. Non-Newtonian Fluid Heat Transfer in Porous Media. Adv Heat Transf. 1994; 24(C):101-90. https://doi.org/10.1016/S0065-2717(08)70233-8
20. Mahapatra N, Dash GC, Panda S, Acharya M. Effects of chemical reaction on free convection flow through a porous medium bounded by a vertical surface. J Eng Phys Thermophys. 2010; 83(1):130-40. https://doi.org/10.1007/s10891-010-0327-1
21. Pal D, Mandal G. Magnetohydrodynamic heat and mass transfer of sisko nanofluid past a stretching sheet with nonlinear thermal radiation and convective boundary condition. J Nanofluids. 2019; (8):852-60. https://doi.org/10.1166/jon.2019.1620
22. Choi, Eastman. Enhancing Thermal Conductivity of Fluids with Nanoparticles. Proceedings of the ASME International Mechanical Engineering Congress and Exposition. 1995; 66:99-105.
23. Rashidi S, Hormozi F, Karimi N, Ahmed W. Applications of nanofluids in thermal energy transport. Emerg Nanotechnologies Renew Energy. 2021; pp. 345-68. https://doi.org/10.1016/B978-0-12-821346-9.00018-3
24. Dukhan N. Forced convection of nanofluids in metal foam: An essential review. Int J Therm Sci. 2023; 187:108156. https://doi.org/10.1016/j.ijthermalsci.2023.108156
25. Bouslimi J, Alkathiri AA, Althagafi TM, Jamshed W, Eid MR. Thermal properties, flow and comparison between Cu and Ag nanoparticles suspended in sodium alginate as Sutterby nanofluids in solar collector. Case Stud Therm Eng. 2022; 39:102358. https://doi.org/10.1016/j.csite.2022.102358
26. Yang L, Zhou F, Sun L, Wang S. Thermal management of lithium-ion batteries with nanofluids and nano-phase change materials: a review. J Power Sources. 2022; 539: 231605. https://doi.org/10.1016/j.jpowsour.2022.231605
27. Moradikazerouni A. Heat transfer characteristics of thermal energy storage system using single and multi-phase cooled heat sinks: A review. J Energy Storage. 2022; 49:104097. https://doi.org/10.1016/j.est.2022.104097
28. Rosseland S. Astrophysik und Atom-Theoretische Grundlagen: Springer, Berlin, Germany. 1931; pp. 41-44. https://doi.org/10.1007/978-3-662-26679-3

Nomenclature

A Sisko fluid parameter/material parameter.
a shear rate viscosity.
b Consistency index of Sisko nanofluid.
B_0 Magnetic induction parameter.
Cp Specific heat capacity at constant pressure (J/KgK).
C Concentration (Kg/m^3).
C_w Nanoparticles wall concentration (Kg/m^3).
C∞ Ambient concentration (Kg/m^3).
Cf_x Skin friction coefficient.
D_T Thermophoretic motion coefficient (m^2/s).
D_B Brownian motion coefficient (m^2/s).
f Dimensionless velocity.
F Forchheimer number.

K Permeability parameter (m^2).
μ Dynamic viscosity (Ns/m^2).
K_r Chemical reaction parameter.
K_1 Porous medium parameter.
K^* Mean absorption Coefficient.
k_f Thermal conductivity(W/mK).
M Magnetic field parameter.
n Power law index.
N_B Dimensionless Brownian motion parameter.
N_T Dimensionless Thermophoresis parameter.
Nu_x Local Nusselt number.
P_r Prandtl number.
q_r Radiative heat flux(W/m^2).
R Thermal radiation.
Re Reynolds number.
Sh_x Local Sherwood number.
T Temperature of the fluid (K).
T∞ Ambient temperature (K).
T_w Wall temperature (K).
u, v Velocity components in x, y directions respectively (m/s).
x Distance along the surface (m).
y Distance perpendicular to the surface (m).
σ Dimensionless chemical reaction parameter.
φ Dimensionless porous medium parameter.
τ Ratio between the effective heat capacitance the nanoparticle material and heat capacitance of the fluid.
χ Dimensionless density of microorganisms.
θ Dimensionless temperature.
α Thermal diffusion coefficient (m^2/s).
P.D. Es Partial differential equations.
O.D. Es Ordinary differential equations.